

Clustering of visible matter and model dark matter halos on different mass and spatial scales

© A.V. Tikhonov^{1,5}, A.I. Kopylov^{2,6}, S. Gottloeber^{3,7}, G. Yepes^{4,8}

¹ Saint-Petersburg State University; ² Special Astrophysical Observatory of RAS, Nizhnii Arkhyz, Karachai-Cherkessian Republic, 369167, Russia;

³ Astrophysical Institute Potsdam, Germany;

⁴ Grupo de Astrofísica, Universidad Autónoma de Madrid;

⁵ Email: ti@hotbox.ru, ⁶ Email: akop@sao.ru, ⁷ Email: sgottloeber@aip.de, ⁸ Email: gustavo.yepes@uam.es

Abstract: We present the investigation of large-scale distribution of galaxy clusters from several X-ray and optical catalogs. Different statistics of clustering like conditional correlation function and cluster analysis (minimal spanning tree (MST) as well as void statistics, which supplement each other, were used. Clusters shows two distinct regimes of clustering: 1) on scales of superclusters ($\sim 40 h^{-1}$ Mpc) that is represented as a power law density decline with distance up to a certain scale; 2) on larger scales a gradual transition to homogeneity ($\sim 100 h^{-1}$ Mpc) is observed. We also present correlation analysis of galaxy distribution from DR6 SDSS main database. For galaxies limiting scales for clustering regimes are 1) $\sim 10 h^{-1}$ Mpc; 2) $\sim 40-50 h^{-1}$ Mpc. We made a comparison of density contrasts of inhomogeneities in cluster and galaxy distributions in the SDSS region. We claim that a value of density contrast should be taken into account to reconcile the observed gradual transition to homogeneity with the apparent presence of structures on corresponding scales. Estimation of relative cluster-galaxy bias give the value $b=5\pm 2$. Differences in characteristic scales and scaling exponents on small scales of cluster and galaxy distribution can be naturally explained in theory of biased structure formation. Distribution of real clusters is compared to that of simulated (model) clusters (the MareNostrum Universe simulation) for WMAP3 cosmological parameters with a higher normalization of the initial power spectrum $\sigma_8 = 0.8$. On the basis of galaxy sample we try to find an approach to reveal the nature of the power law behavior showed by the conditional correlation function on small scales. We show that this phenomenon is quite complex, with significant scatter in scaling properties, and characterized by non-trivial dependence on galaxy properties and environment. We made an attempt to associate the exponent of power law of the conditional correlation function with the contrast of structures observed in distribution of galaxies. Our results show that properties of the power law clustering on small scales can not be adequately described by such simple models as a pure fractal one.

1. Introduction

Clusters of galaxies are the most massive virialised structures in the Universe. Within the framework of the modern “picture of the world” with dark matter and dark energy (cosmological constant) the structures evolve via gravitational instability starting from small seeds which are described by the spectrum of initial inhomogeneities. Clusters of galaxies are perfect probes of the matter distribution on large scales. Studying their spatial distribution one can constrain the parameters of the Λ CDM model (Ω_m , σ_8). Baryonic gas falls into cluster potential wells and heats up to temperatures of order of 10^7 K so that it emits X-rays. Clusters of galaxies were historically identified first as overdensities in the galaxy distribution (ACO [1] and APM [2] optical galaxy cluster catalogs). This kind of selection gives some amount of spurious objects due to projection effects. When clusters are detected according to their X-ray flux we undoubtedly deal with deep potential wells. In this work we investigated the distribution of galaxy clusters selected by X-ray flux from several catalogs of X-ray clusters and compare it with simulated clusters taken from the “MareNostrum Universe” [3].

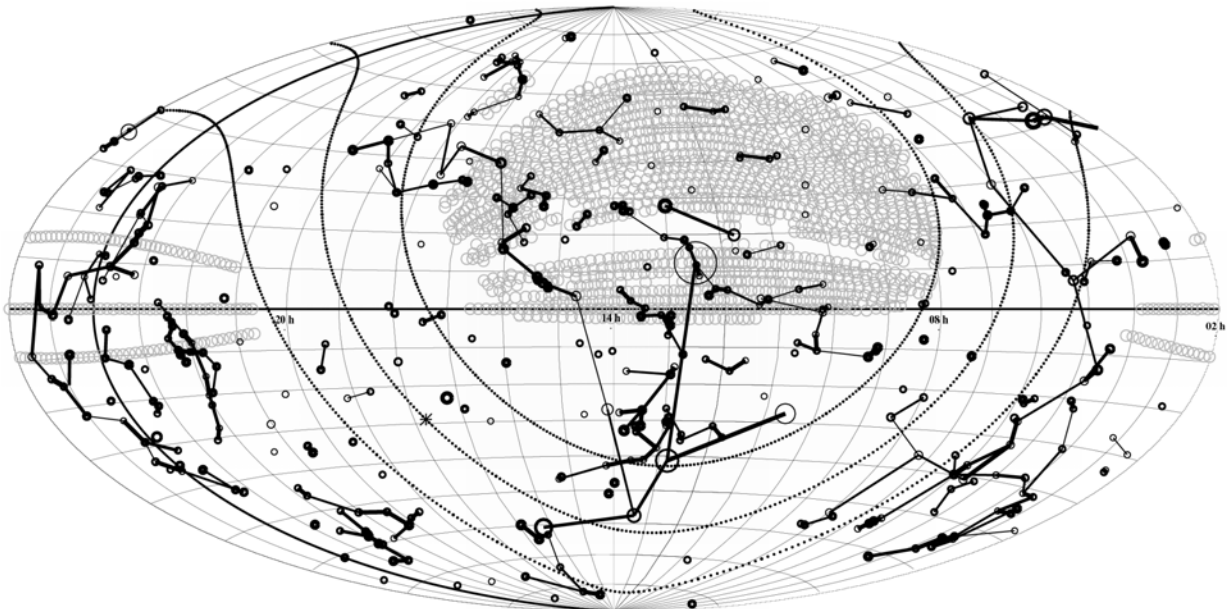


Fig. 1. Distribution in equatorial coordinates of 400 X-ray clusters with $z < 0.1$ and $L_x(0.1-2.4 \text{ keV}) > 1.25 \cdot 10^{43} \text{ h}^{-2} \text{ erg/s}$. The edges of minimal spanning tree shorter than $45 \text{ h}^{-1} \text{ Mpc}$ are shown by solid lines. Circles of constant galactic latitude ($b = -20^\circ, 0^\circ, +20^\circ$) are plotted by dotted lines. Gray circles represent the spectral plates of the SDSS-DR6.

2. X-ray clusters

The X-ray cluster sample consist of the all sky ROSAT clusters with X-ray flux $F_x \geq 3 \cdot 10^{-12} \text{ erg/cm}^2/\text{s}$ in the (0.1-2.4 keV) energy band. Clusters were selected from the following catalogs: 1) REFLEX (N=186 clusters) [4]; eBCS (N=108) [5,6]; NORAS (N = 36) [7]; CIZA (N = 70, galactic latitude $|b_{\text{gal}}| < 20^\circ$) [8,9]. The final all-sky sample consists of 400 X-ray clusters up to redshift $z < 0.1$ with luminosity $L_x > 1.25 \text{ h}^{-2} \cdot 10^{43} \text{ erg/s}$ (assuming the current rate of universal expansion - Hubble constant $H_0 = 100 \text{ km/s/Mpc}$, $h = H/H_0$, where H is the true value of Hubble constant). The volume-limited sample (VL) extracted from this compilation contains 233 X-clusters with redshifts limited by $Z_{\text{VL}} = 0.09$ (which corresponds to the radial distance of $265.3 \text{ h}^{-1} \text{ Mpc}$ ($\Omega_m = 0.24$, $\Omega_\Lambda = 0.76$) with $L_x > 2.5 \text{ h}^{-2} \cdot 10^{43} \text{ erg/s}$).

3. Model clusters

The MareNostrum clusters (MN-clusters) were extracted from the $500 \text{ h}^{-1} \text{ Mpc}$ simulation box MUWHS [10] with cosmological parameters $\Omega_m = 0.24$, $\Omega_\Lambda = 0.76$, $h = 0.73$, $\sigma_8 = 0.8$ (σ_8 , the present-day rms mass fluctuations on spheres of radius $8 \text{ h}^{-1} \text{ Mpc}$ is slightly higher than predicted by WMAP3 and in better agreement with WMAP5). Within a box of $500 \text{ h}^{-1} \text{ Mpc}$ size the linear power spectrum at redshift $z = 40$ has been represented by 512^3 DM particles of mass $m_{\text{DM}} = 8.3 \cdot 10^9 \text{ h}^{-1} M_{\text{sun}}$ (**further we assume $h=1$**). The nonlinear evolution of structures has been followed by the GADGET II code of V. Springel [11]. Clusters were identified in the simulation by the FOF (friend-of-friend) algorithm. For comparison with observations we extracted the 233 most massive clusters from a sphere of radius 265.3 Mpc (we slightly expanded the simulation box using the periodic boundary conditions). We choose the simulated sample by keeping its number density equal to the observed cluster density (independent of an $L_x - \text{mass}$ relation) so that the most massive simulated cluster corresponds to the most luminous observed clusters. We use the 3D velocities of the simulated clusters and place an observer to the center of the sphere extracted from the simulation box. Then the cluster positions were converted to redshift space. The mass of the lightest dark matter cluster in the simulated sample is $2.46 \cdot 10^{14} M_{\text{sun}}$.

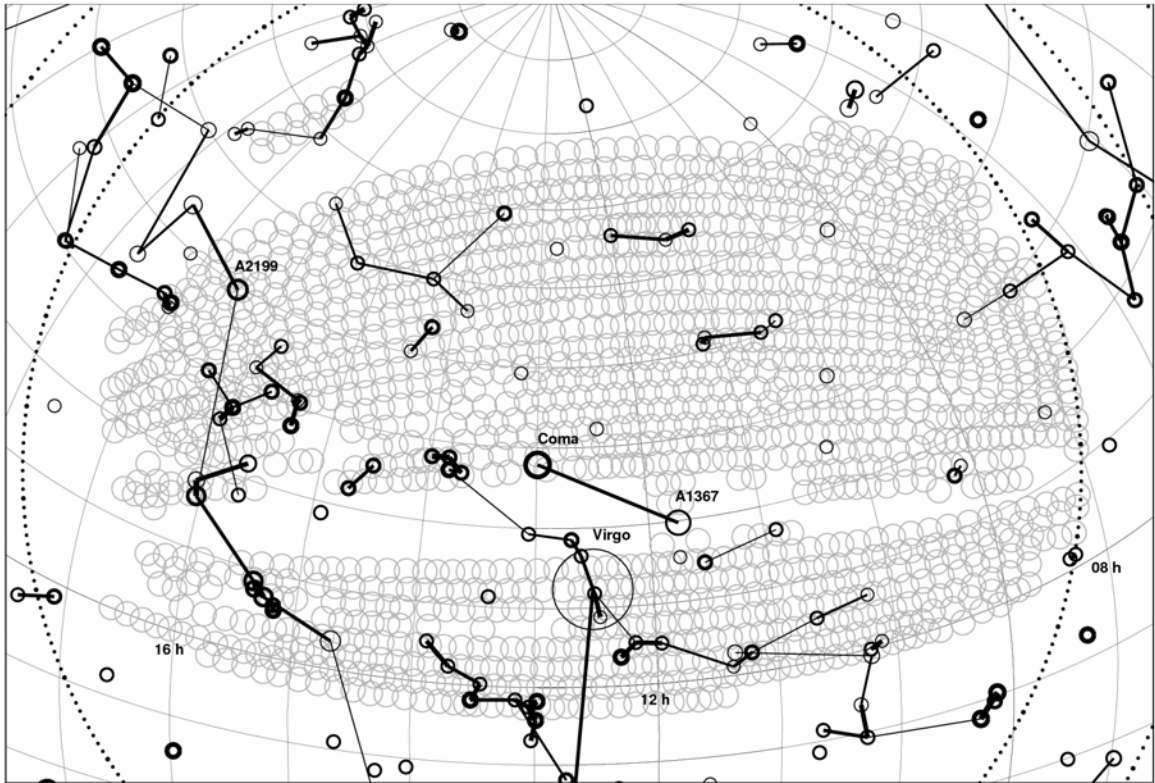


Fig. 2. Distribution of X-ray clusters with $z < 0.1$ and $L_x(0.1-2.4 \text{ keV}) > 1.25 \cdot 10^{43} \text{ h}^{-2} \text{ erg/s}$ around the Northern Galactic Pole. The edges of minimal spanning tree shorter than $45 \text{ h}^{-1} \text{ Mpc}$ are shown by solid lines. Circles of constant galactic latitude ($b = 0^\circ, +20^\circ$) are plotted by dotted lines. Gray circles represent the spectral plates of the SDSS-DR6.

4. Statistics of clustering

4.1. Conditional correlation function

In order to compare the X-ray and simulated cluster distributions we use different statistical methods. The conditional correlation function (CCF) [12,13] measures (by averaging from all clusters which take part in analysis as centers of spheres with given working radius) the mean trend of density measured in spheres (integral CCF). The clusters show three distinct regimes of clustering (Fig.3a): 1) on scales of superclusters the CCF is represented by a power law density decline up to a scale of 35-40 Mpc; 2) on larger scales a gradual transition to homogeneity is observed; 3) starting from about 100 Mpc the CCF stays constant, i.e. the number density does not anymore decline with increasing radius of spheres. Fluctuations on scales > 100 Mpc exist but here we reach a mean number density of clusters (which is not defined on smaller scales).

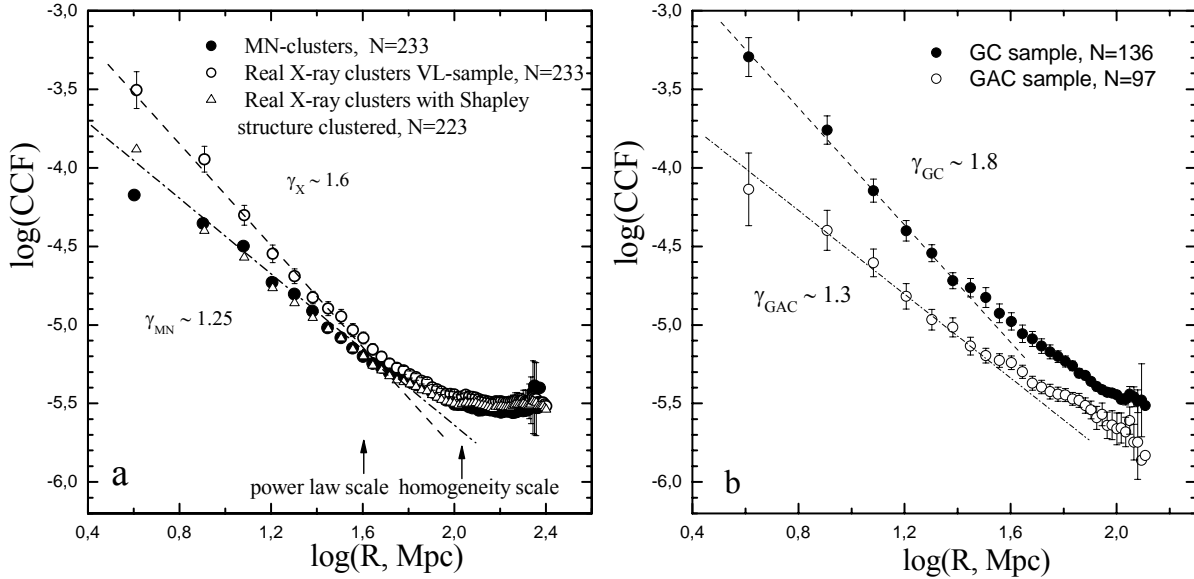


Fig. 3. a) Comparison of CCFs for X-clusters and MN-clusters; b) CCFs for VL cluster sample in 2 hemispheres: GAC ($123^0 < l_{gal} < 303^0$) and GC ($303^0 < l_{gal}$ and $l_{gal} < 123^0$).

The CCFs for observed and simulated clusters look quite similar (the second regime of clustering from ~ 40 to ~ 100 Mpc is perfectly reproduced by the simulated clusters) however the value of the slopes on scales below 40 Mpc are different: $\gamma_X \sim 1.6$ for the observed and $\gamma_{MN} \sim 1.25$ for the simulated clusters. This difference reflects the lack of close pairs in the simulated cluster distribution with respect to the observed ones. The comparison with a model cluster distribution obtained from the same realization but using a smaller linking length of the FOF algorithm (in order to identify substructure and possible close pairs which could be linked by the original linking length) showed that FOF parameters have negligible influence on the value of the slope. In order to understand the difference in the slopes we have gathered observed cluster pairs with separations smaller than 5 Mpc into single objects. This reduces the total number of objects in the observed sample by 10. Mostly the clusters that belong to the Shapley supercluster (located at $l_{gal} \sim 311^0$, $b_{gal} \sim +30^0$ and redshift $z \sim 0.05$) (Fig.6) were linked. The CCF of the reduced sample (Fig.3a) looks nearly identical to the simulated one (γ_{MN} is very close to the γ_X of the reduced observational sample). When we calculate CCF separately in two hemispheres we obtain the value of slope γ_{GAC} very close to the model γ_{MN} in the GAC hemisphere that doesn't contain the Shapley supercluster (Fig.3b). This means that the difference is mainly produced by the Shapley supercluster - we don't have such a structure in the simulated cluster sample. It is an open question how often such outstanding structures appear in the Universe and whether they can be reproduced by Λ CDM simulations of larger volumes which should contain larger wavelength perturbations that could be responsible for formation of more massive objects.

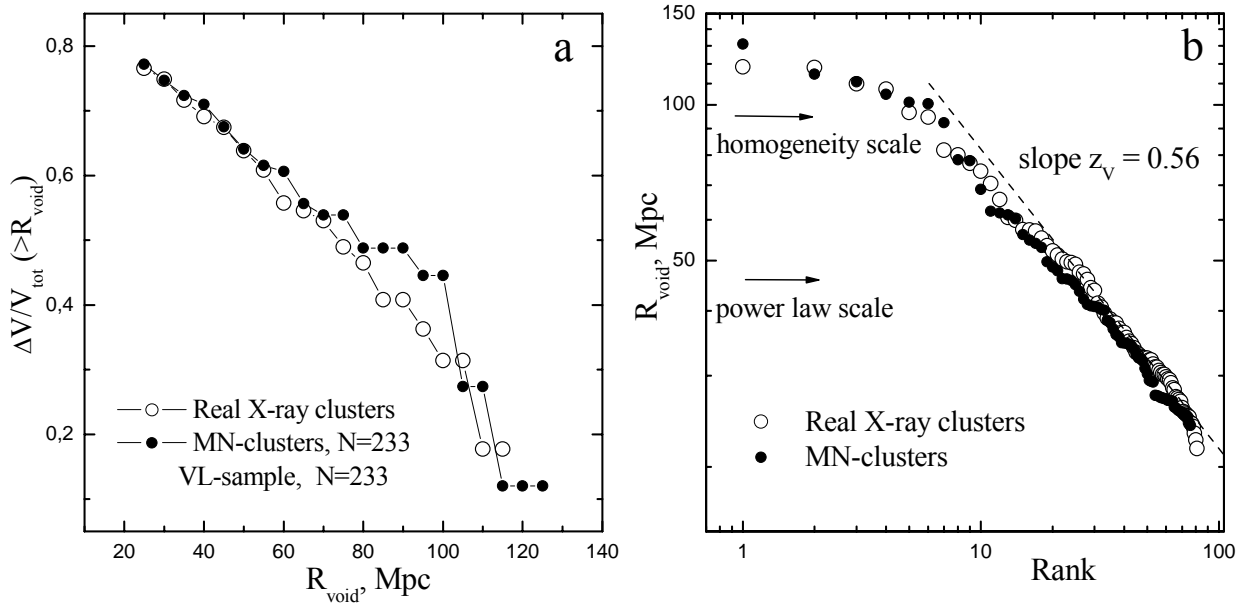


Fig. 4. a) CVF for X-ray and model MN-clusters; b) DVF for X-ray and model MN-clusters.

4.2. Void statistics

We have also performed a void analysis of the same observed and simulated samples. Starting from the largest empty spheres non-spherical voids have been constructed by extending the original spherical void with empty spheres of smaller radii the center of which was inside the original void. The radius of the smaller spheres is limited to be larger than an *ad hoc* parameter 0.9 of the radius of initial sphere. The process is repeated a few times. It produces voids which are slightly non-spherical. The mean distance between the observed (and simulated) clusters is ~ 28 Mpc. Therefore, we have limited our voids to a minimal radius of 20 Mpc. The cumulative void functions (CVF) $\Delta V/V_{\text{sample}}$ show that the observed and simulated voids fill the sample volumes in a similar way though in Fig.4a we see a difference at $R_{\text{void}} \sim 80$ Mpc: the largest simulated voids are bigger than the observed ones. Here the differential VF is presented as R_{void} versus rank ($R_{\text{void}} = (3V_{\text{void}}/4\pi)^{1/3}$). It shows rather good agreement between observation and simulation. There are two breaks in the DVF (Fig.4b). The one at $R_{\text{void}} \sim 45$ Mpc is associated with the scale where the power law regime of clustering vanishes. The break at $R_{\text{void}} \sim 100$ Mpc can be directly associated with the scale of homogeneity. The slope of the R_{void} -Rank relation after the break is $z_V = 1/(3-\gamma_{\text{voids}})$ which gives $\gamma_{\text{voids}} \sim 1.2$ close to the slope of the CCF on small scales.

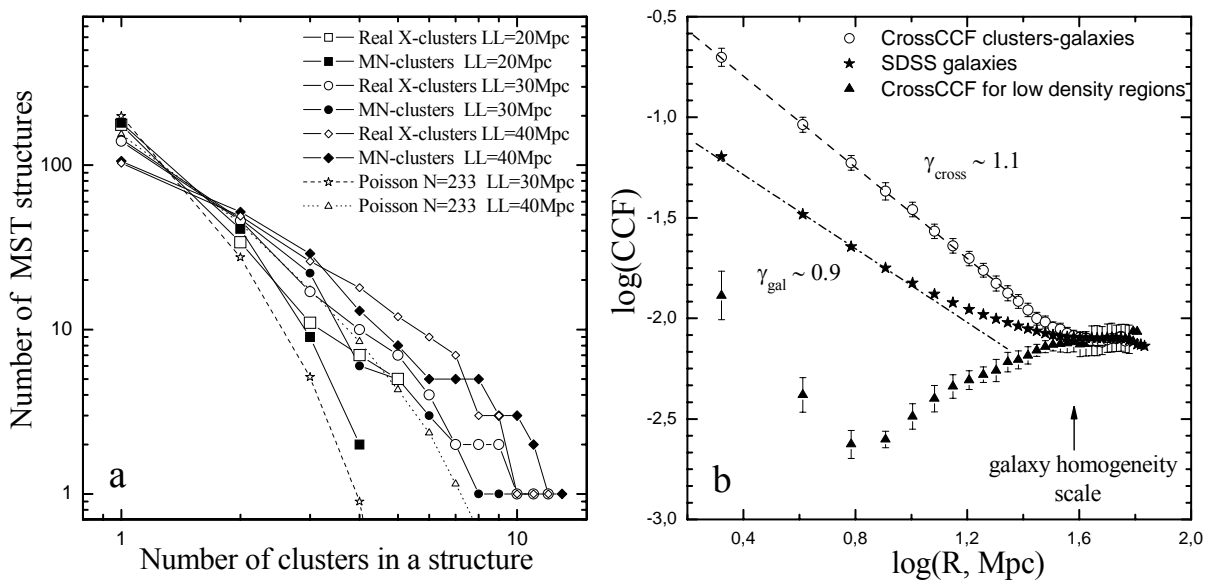


Fig. 5. a) MST analysis for X-ray and model MN-clusters; b) CrossCCF clusters-galaxies (open circles), CCF of SDSS galaxies (stars; error bars are smaller than symbol size), low density region galaxies crossCCF (triangles, 10 realizations).

4.3. Cross-correlation of clusters and galaxies

From SDSS DR6 main galaxy database we selected region in galactic coordinates ($48^0 < l_{\text{gal}} < 210^0$, $50^0 < b_{\text{gal}} < 86^0$) and built the VL sample with $z_{\text{max}}=0.1$ and $M_{\text{lim}} = -19.67$ (see section 5). There are 23 X-clusters from our compilation in this region. In Fig.5b we present clusters-galaxies cross-CCF (clusters were used as centers of spheres where number of galaxies was calculated) in comparison with CCF of SDSS galaxies in selected region (stars in Fig.5b). We defined local number galaxy contrast $\Delta = 11/(4\pi R_{10}^3/3)/\rho_{\text{mean}} - 1$, where R_{10} – distance to 10th neighbour (mean $R_{10} \sim 4\text{Mpc}$ for entire sample), ρ_{mean} – mean galaxy number density in the sample. In this sense clusters located in the sample have the median $\Delta \sim 40$. We selected randomly 23 galaxies separated by more than 10 Mpc with $\Delta < 0$ (10 realizations) which are located in void regions and calculated the mean cross CCF for low density regions (filled triangles Fig.5b). We see the same scale of plateau on CCF ~ 40 Mpc independently of the way of calculation. Cluster-galaxy cross-CCF shows stronger correlation than is observed in entire galaxy population (CCF of SDSS galaxies) and inherits from cluster-cluster correlations the length of scaling regime. Note that all three curves on Fig.5b, calculated in rather different ways, converge to homogeneity regime on the same scale of ~ 40 Mpc.

4.4. Minimal Spanning Tree

We built minimal spanning trees (MST) of the samples. The MST consists of knots and edges and is constructed by appending new knots satisfying the condition for the distance to the already constructed part of the tree being at a minimum [14]. The MST and void analysis give us a clue to outline the "skeleton" of structures represented by clusters. The full length of the truncated MST when only knots having more than 1 edge left, normalized to the number of such knots is $L_{\text{tr}}^{\text{X}} = 37$ Mpc for the X-ray cluster sample and $L_{\text{tr}}^{\text{MN}} = 38$ Mpc for the simulated sample (for comparison, random samples with the same number density give after averaging $L_{\text{tr}}^{\text{R}} = 47$ Mpc). Using the MST linking lengths $\text{LL}=20$, $\text{LL}=30$ and $\text{LL}=40$ Mpc we have constructed the cumulative functions of structure abundances (Fig.5a) for the observed, simulated and randomly generated samples. Clusters in the observed sample are slightly more structured than the simulated ones (largest differences are for $\text{LL}=20$ Mpc – effect of discussed (section 4.1) lack of close pairs in the simulated sample) but the largest structures in both samples (for $\text{LL}=30$ and 40 Mpc) have nearly the same number of clusters: we see overall agreement of abundances of observed and simulated structures detected on a chosen levels of connectivity. Again we see large deviation from the Poisson sample results for both values of LL which is another signature of clustering in our samples.

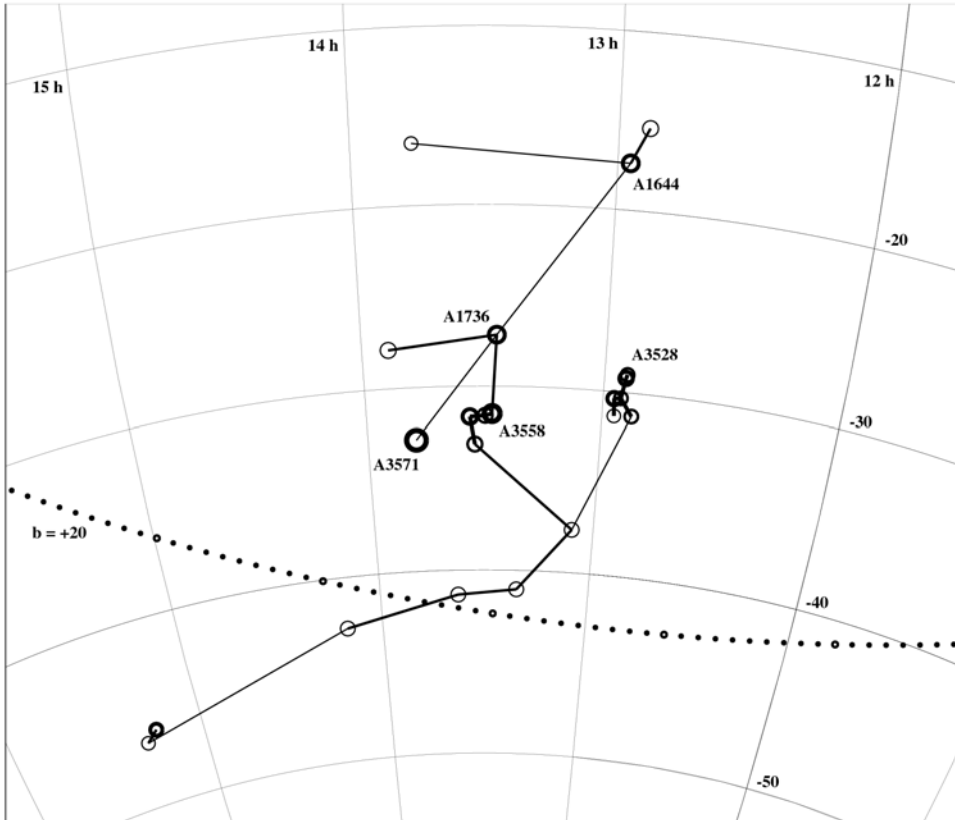


Fig. 6. X-ray luminous ($L_x(0.1-2.4 \text{ keV}) > 1.25 \cdot 10^{43} \text{ h}^{-2} \text{ erg/s}$) member clusters of Shapley supercluster ($0.039 < z < 0.059$) connected by the edges of minimal spanning tree shorter than $40 \text{ h}^{-1} \text{ Mpc}$.

5. CCF of galaxy samples from SDSS DR6 main galaxy database

When analyzing the SDSS DR6 data, we selected 3 rectangular regions from the region of spectroscopic sky coverage for the convenience of allowance for the boundary conditions for CCF and for ensuring sample completeness. In the (λ, η) coordinate system of the survey, the selected regions are S1: $-48^\circ < \lambda < 30^\circ$, $-6^\circ < \eta < 35^\circ$; S2: $-25^\circ < \lambda < 48^\circ$, $6^\circ < \eta < 35^\circ$; S3: $-54^\circ < \lambda < -16^\circ$, $-33^\circ < \eta < -17^\circ$.

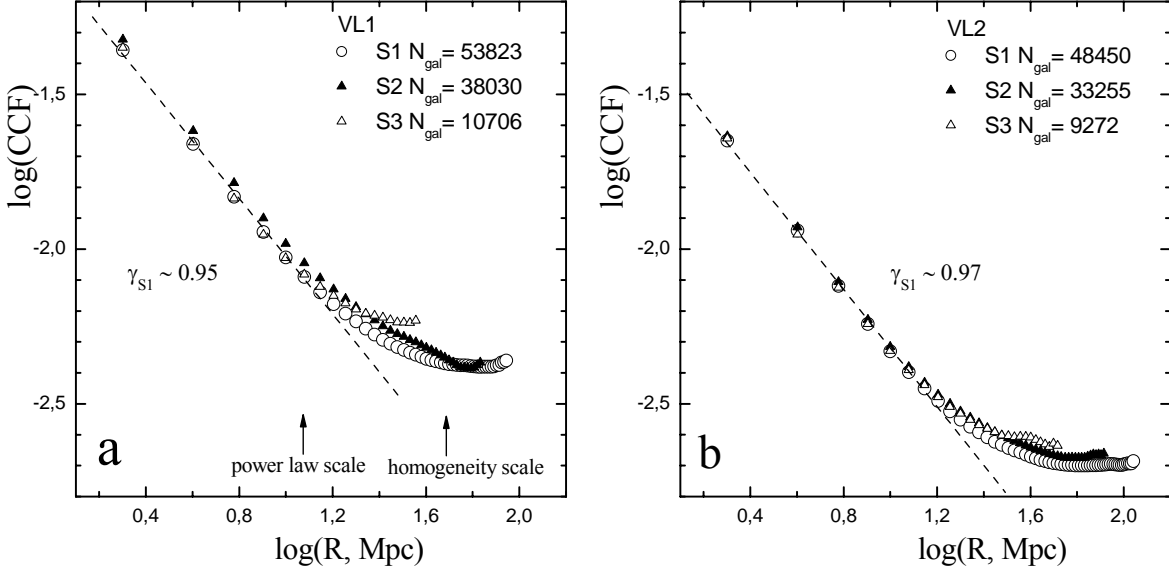


Fig.7. CCFs for different VL samples from DR6 SDSS main galaxy database. N_{gal} – number of galaxies in a sample.

Then we constructed VL samples to eliminate incompleteness in radial coordinate: we set the limit on the r -band absolute magnitude M_r for the sample galaxies equal to $M_{\text{lim}} = r_{\text{lim}} - 25 - 5 \log(R_{\text{max}}(1 + z_{\text{max}})) - K(z)$, where $r_{\text{lim}} = 17.77$ was taken as the limiting r -band magnitude, $K(z)$ is the K -correction, and R_{max} is the chosen far boundary in radial coordinate corresponding to z_{max} (for $\Omega_\Lambda = 0.7$, $\Omega_0 = 0.3$). So we have in VL-sample all galaxies with $M_r < M_{\text{lim}}$. The r magnitudes used here were corrected for extinction. To estimate the absolute magnitudes of the galaxies, we used an approximation for K -correction for SDSS galaxies in the form $K(z) = 2.3537z^2 + 0.5735z - 0.18437$ [15,16]. We present results for two cuts on redshift (z_{max}): VL1 ($z_{\text{max}} = 0.12$, $M_{\text{lim}} = -20.11$) and VL2 ($z_{\text{max}} = 0.15$, $M_{\text{lim}} = -20.68$) (Fig7a,b). CCF method deal with spheres fully included in a sample so for large radii centers of spheres tend to locate close to each other and we limited our analysis to the scale defined by condition that spheres of large radii do not overlap by more than half of their volumes. Power law regime is limited by scales ~ 10 -15 Mpc and CCFs of different samples show rather concerted convergence to homogeneity regime. We should note small but distinct differences in amplitudes of homogeneous regime of CCFs for three different regions. This mean that on such scales we can measure mean density with some scatter that is caused by cosmic variance, i.e. the presence of different structures in different samples. Characteristic scales of galaxy correlations are significantly smaller than ones produced by clusters in proportions that are similar to those obtained by early application of traditional two-point correlation function $\xi(r)$ (see e.g. [17]). These differences has natural explanation in the theory of biased structure formation.

6. Estimation of relative cluster-galaxy bias on 200 Mpc scale

Theory of structure formation predicts that clustering of most massive dark matter halos (clusters) is enhanced relative to that of the general mass distribution (galaxies) [18, 19]. Fig.1 shows large inhomogeneities on scales 100-300 Mpc in distribution of clusters. In the northern region of SDSS (Fig.2) we can estimate relative clustering bias (b) for volume-limited samples of clusters with $L_X \geq 2.5 \cdot 10^{43}$ erg/s and galaxies with $M_r < -19.67$. In three equal volumes of $5.2 \cdot 10^6 \text{ Mpc}^3$ defined in redshift intervals 0.020-0.069, 0.069-0.087 and 0.087-0.100 for the area covered by the SDSS-DR6 spectral survey (≈ 6100 square degrees) there are 12, 32 and 13 clusters and 36612, 46785 and 38566 galaxies, respectively. These counts give a rough estimate of cluster-galaxies relative bias $b = 5 \pm 2$ on the scale 200 Mpc. This estimate is consistent with the bias ($b = 3$) measured for massive halos ($\sim 3 \cdot 10^{14} M_{\text{sun}}$) in N-body simulations, but on

scales 15-30 Mpc [20].

7. Scaling properties of galaxies

Galaxy integral CCF shows power low up to scales ~ 10 -15 Mpc with exponent $\gamma_{\text{gal}} \sim 1.0$ (see section 5) for samples containing galaxies with absolute magnitudes less than M^* (more luminous than M^* galaxies tend to be more clustered [13, 21, 22]). For investigation of scaling properties of individual galaxies on such scales we chose all galaxies from the sample (section 5) VL1-S1 ($z_{\text{max}} = 0.12$) that located from sample boundaries on more than 10 Mpc. We calculated individual Number-Radius relation (number of galaxies in a sphere in dependence on sphere radius $R_{\text{sp}} \leq 10$ Mpc) for each galaxy by using linear approximation with slope s_{NR} of $\log(N)$ - $\log(R)$ dependence. We excluded from analysis very isolated galaxies and galaxies that have the error of slope σ_s more than 0.3 (taking into account dispersion of slope values): about 37000 galaxies left. Surprisingly the mean slope $s_{\text{NR}}^m = 1.7$ (which also corresponds to the maximum in the histogram of slope values) does not correspond to exponent $\gamma_{\text{SI}} \sim 1.0$ of CCF of the sample on scales ~ 10 Mpc (for example in homogeneous scale-invariant distribution it should be $s_{\text{NR}}^m = 3 - \gamma_{\text{CCF}}$). Dispersion of slopes distribution is significant: $\sigma_{\text{NR}} = 0.6$. We went to conclusion by defining galaxy structures according to their contrast and connectivity (using MST technigue) that it is hard to associate galaxies with slopes in certain narrow range with identified structures – there is complex mix of slopes with significant dispersion, but the existence of possibility to trace structures by their scaling properties is still an opening question. There is some amount of slopes $s_{\text{NR}} > 3$: all of them are associated with galaxies in relatively low density regions with $\Delta < 10$ (value of local contrast defined in section 4.3). Following the approach of [23] we performed multiscaling analysis that weights high and low density regions in different way according to the positive or negative counts-weighting exponent $q-1$. Generalized dimensions D_q differs significantly for different values of q (D_q increases from $D_{.4} = 1.1$ to $D_2 = 1.8$) which is another signature of complexity of scaling properties on small scales: usually this effect is interpreted as a manifestation of multifractality. It is evident that galaxy large scale structure on small scales can not be described by simple models like ones with unique scaling exponent.

8. Conclusions

Application of different complementary statistics to samples of observed and simulated clusters of galaxies, chosen in a way to fit the observed number density of the volume limited X-ray cluster sample, show general agreement in the distribution of most massive virialised objects in the Universe and in cosmological simulations. Based on the CCF we found the same scale (~ 100 Mpc) of statistical homogeneity (in a sense that we have a definite (but fluctuating) mean number density of objects on such scales) for observed and simulated clusters (this scale can be related to the comoving scale of the largest wavelength of acoustic oscillation of the photon-baryon plasma before recombination [24]). Very interesting is the coincidence of the second (transitional) clustering regime (beyond the characteristic scale of superclusters) shown both by the observed and simulated CCF on scales 40-100 Mpc. The Shapley supercluster strongly affects the value of the CCF slope of clusters on small scales and it is responsible for the differences in distribution characteristics of observed and simulated clusters: we see a lack of close massive cluster pairs in simulations. Larger boxes are necessary to find such outstanding structures in simulations. The MST analysis shows that the observed clusters are slightly more structured than the simulated ones. In summary, the distribution of most massive Λ CDM halos of dark matter show a reasonable agreement with the distribution of most luminous X-ray clusters of galaxies. Significant differences in characteristic scales of distribution of X-ray clusters and SDSS galaxies (power low scales are 40 Mpc and 10Mpc and homogeneity scales are 100 and 40-50 Mpc respectively) are similar to differences obtained in early works by using two-point correlation function and can be explained by theory of biased structure formation. Our estimation of relative cluster-galaxy bias value ($b \sim 5$) is in general agreement with theoretical prediction. Power low behaviour of decline of galaxy density with distance indicated by CCF (correlation exponent γ) on small scales has a very complex nature: dependence of γ on colors and luminosities of galaxies, significant scatter of individual exponents of number-radius relation for different galaxies in a sample, evidences of multifractality – differences in scaling properties according to an environment (high and low density regions).

Acknowledgements

This research was supported in part by the Russian Foundation for Basic Research (grant 07-02-

01417a). Work of A.V. Tikhonov was supported by ASTROSIM (short visit grant 2089). A.V. Tikhonov thanks German service DAAD for possibility to work in Astrophysical Institute Potsdam. This research has made use of the NASA/IPAC Extragalactic Database (NED). The creation and distribution of the SDSS Archive has been funded by the Alfred P. Sloan Foundation, the Participating Institutions, the National Aeronautics and Space Administration, the National Science Foundation, the US Department of Energy, the Japanese Monbukagakusho, and the Max Planck Society. The SDSS Web site is <http://www.sdss.org/>.

References

- [1] G.O. Abell, H.C. Corwin and R.P. Olowin, A catalog of rich clusters of galaxies, // *ApJ. Suppl. Ser.*, Vol. 70, p. 1. (1989).
- [2] G.B. Dalton, S.J. Maddox, W.J. Sutherland, G. Efstathiou, The APM Galaxy Survey - V. Catalogues of galaxy clusters // *MNRAS*, Vol. 289, p. 263 (1997).
- [3] S. Gottlöber, G. Yepes, Shape, spin and baryon fraction of clusters in the MareNostrum Universe // *ApJ*, Vol. 664, p. 117 (2007).
- [4] H. Bohringer, P. Schuecker, L. Guzzo et al., The ROSAT-ESO Flux Limited X-ray (REFLEX) Galaxy cluster survey. V. The cluster catalogue // *Astronomy & Astrophysics*, Vol. 425, p. 367 (2004).
- [5] H. Ebeling, A.C. Edge, H. Bohringer et al., The ROSAT Brightest Cluster Sample - I. The compilation of the sample and the cluster log N-log S distribution // *MNRAS*, Vol. 301, p. 881, (1998).
- [6] H. Ebeling, A.C. Edge, S.W. Allen et al., The ROSAT Brightest Cluster Sample - IV. The extended sample // *MNRAS*, Vol. 318, p. 333 (2000).
- [7] H. Bohringer, W. Voges, J.P. Huchra et al., The Northern ROSAT All-Sky (NORAS) Galaxy Cluster Survey. I. X-Ray Properties of Clusters Detected as Extended X-Ray Sources // *ApJ Supplement*, Vol. 129, p. 435 (2000).
- [8] H. Ebeling, C.R. Mullis and R.B. Tully, A Systematic X-Ray Search for Clusters of Galaxies behind the Milky Way // *ApJ*, Vol. 580, p. 774 (2002).
- [9] D.D. Kocevski, H. Ebeling, C.R. Mullis and R.B. Tully, A Systematic X-Ray Search for Clusters of Galaxies behind the Milky Way. II. The Second ClZA Subsample // *ApJ*, Vol. 662, p. 224 (2007).
- [10] G. Yepes, R. Sevilla, S. Gottlöber, J. Silk, Is WMAP3 normalization compatible with the X-ray cluster abundance? // *ApJ Letters*, Vol. 666, p. L6 (2007).
- [11] V. Springel, The cosmological simulation code GADGET-2 // *MNRAS*, Vol. 364, p. 1105 (2005).
- [12] Tikhonov, A. V.; Makarov, D. I.; Kopylov, A. I., Investigation of clustering of galaxies, clusters and superclusters by the method of correlation Gamma-function // *Bulletin of the Special Astrophysical Observatory of RAS*, Vol. 50, p. 39; (2000) arXiv:astro-ph/0106276.
- [13] A. V. Tikhonov, Correlation properties of galaxies from the Main Galaxy Sample of the SDSS survey // *Astronomy Letters*, Vol. 32, p. 721 (2006); arXiv:astro-ph/0610643.
- [14] J. Barrow, S. Bhavsar, and D. Sonoda, Minimal spanning trees, filaments and galaxy clustering // *MNRAS*, 1985, Vol. 216, p.17.
- [15] C. Hikage et al., Fourier Phase Analysis of SDSS Galaxies // *PASJ*, Vol. 57, p. 709, (2005).
- [16] M. Blanton, J. Brinkmann, I. Csabai et al., Estimating Fixed-Frame Galaxy Magnitudes in the Sloan Digital Sky Survey // *Astron. J.* **125**, 2348 (2003).
- [17] A.A. Klypin, A.I. Kopilov, Pis'ma v *Astronomicheskii Zhurnal* // Vol. 9, No. 2, p. 75 (1983) (in Russian).
- [18] N. Kaiser, On the spatial correlations of Abell clusters // *ApJ*, Vol. 284, p. L9 (1984).
- [19] R.K. Sheth, G. Tormen, Large-scale bias and the peak background split // *MNRAS*, Vol. 308, p. 119 (1999)
- [20] A.R. Wetzel, J.D.Cohn, M. White et al., The clustering of massive halos // *ApJ*, Vol. 656, p. 139 (2007)
- [21] Zehavi I., Zheng Z., Weinberg D. et. al., The Luminosity and Color Dependence of the Galaxy Correlation Function // *ApJ.*, Vol. 630, p. 1, (2005)
- [22] A. V. Tikhonov, Voids in the SDSS Galaxy Survey // *Astronomy Letters*, Vol. 33, No. 8, p. 499 (2007).
- [23] P. Grassberger and Procaccia I., Characterization of strange attractors // *Phys. Rev Letters*, 50, 346, (1983)
- [24] D. J. Eisenstein, I. Zehavi, D. W. Hogg et al., Detection of the Baryon Acoustic Peak in the Large-Scale Correlation Function of SDSS Luminous Red Galaxies // *ApJ*, Vol. 633, p. 560 (2005); arXiv:astro-ph/0501171.